Novel Hot-Spot Ignition Designs for Inertial Confinement Fusion with Liquid-Deuterium-Tritium Spheres

V. N. Goncharov, I. V. Igumenshchev, D. R. Harding, S. F. B. Morse, S. X. Hu, P. B. Radha, D. H. Froula, S. P. Regan, T. C. Sangster, and E. M. Campbell
Laboratory for Laser Energetics, University of Rochester, Rochester, New York 14623, USA

(Received 10 February 2020; accepted 10 July 2020; published 5 August 2020)

A new class of ignition designs is proposed for inertial confinement fusion experiments. These designs are based on the hot-spot ignition approach, but instead of a conventional target that is comprised of a spherical shell with a thin frozen deuterium-tritium (DT) layer, a liquid DT sphere inside a wetted-foam shell is used, and the lower-density central region and higher-density shell are created dynamically by appropriately shaping the laser pulse. These offer several advantages, including simplicity in target production (suitable for mass production for inertial fusion energy), absence of the fill tube (leading to a more-symmetric implosion), and lower sensitivity to both laser imprint and physics uncertainty in shock interaction with the ice-vapor interface. The design evolution starts by launching an ~1-Mbar shock into a DT sphere. After bouncing from the center, the reflected shock reaches the outer surface of the sphere and the shocked material starts to expand outward. Supporting ablation pressure ultimately stops such expansion and subsequently launches a shock toward the target center, compressing the ablator and fuel, and forming a shell. The shell is then accelerated and fuel is compressed by appropriately shaping the drive laser pulse, forming a hot spot using the conventional or shock ignition approaches. This Letter demonstrates the feasibility of the new concept using hydrodynamic simulations and discusses the advantages and disadvantages of the concept compared with more-traditional inertial confinement fusion designs.

DOI: 10.1103/PhysRevLett.125.065001

The conventional hot-spot ignition scheme in the inertial confinement fusion (ICF) approach [1,2] uses relatively thin spherical shells of frozen DT fuel overcoated with an ablator material (such as plastic or high-density carbon). These shells are driven by either direct laser illumination [laser direct drive (LDD)] or by x rays emitted from a high-Z enclosure or hohlraum [laser indirect drive (LID)]. Although significant progress in target performance has been demonstrated in both LDD and LID approaches over the last several years [3,4], achieving ignition conditions in ICF implosions remains challenging. Several mechanisms are currently being hypothesized to be responsible for the performance degradation [5]. These include shell nonuniformity growth and mix seeded by target imperfections, target mounts, and the fill tube, and various deviations from spherical symmetry due to either engineering features or DT ice-layer asymmetries. In addition, uncertainty in modeling key implosion physics limits the ability to accurately design low-adiabat, high-convergence implosions.

The thin-shell cryogenic targets currently used in ICF ignition experiments have several disadvantages. First, fabrication of highly uniform frozen DT layers is time consuming and, in some cases, not reproducible. The layer must be sufficiently uniform to prevent seeding the Rayleigh-Taylor (RT) instability [6] developed during shell acceleration [7]. Even though the beta-layering technique [8] optimized over the last decade has produced smoothness that meets the uniformity specification, the layering process and layer quality characterization is still time consuming and different engineering features (such as fill tubes, stalks, and characterization windows in the hohlraum) affect the ice-layer uniformity and cause degradation in target drive symmetry, leading to reduction in target performance. Second, the physics of relatively strong shocks (a few megabars) interacting with solid material (ablator and DT ice) is not well known. For example, the material phase transition behind the shock could lead to chunks of different phases being present in the shocked ablator and fuel, which contributes to the nonuniformity seeding at the ablator-ice interface and the inner surface of the shell as the first shock breaks out of the shell and material starts to accelerate, forming rarefaction or release. In addition, the physics of spallation or jetting of material from the inner ice surface after shock breakout of the shell is also not well understood and its effect on target performance remains uncertain. Third, laser imprint plays a critical role in determining the nonuniformity seeding in the LDD designs [9,10]. Prior to establishing a conduction zone (a region between where the laser energy is deposited and the ablation front) sufficiently large to smooth out the most-damaging modes (typically, these include mode numbers $\ell > 10$), the

nonuniformities seeded by laser beam speckles imprint on the target surface [11]. These amplify due to RT instability during acceleration that starts soon after the first shock breaks out of the shell.

Most of these shortcomings can be addressed by imploding a liquid DT sphere inside a wetted-foam shell. These do not require fill tubes (the capillary forces are great enough to hold the fuel within the foam) and fuel layering, do not have solid (or liquid)-gas interfaces, and have low acceleration during shock propagation through the sphere, preventing significant amplification of early laser imprint and target imperfections. Homogeneous DT spheres have been considered in the past for the volume ignition approach [2]. Volume ignition relies mainly on minimizing radiation losses. Such designs require either high-Z shells to trap radiation in the fuel or a large, optically thick fuel mass. The radiation trapping scheme received significant attention in recent publications [12–14], but the neutron yields predicted in the volume ignition ICF approach do not significantly exceed gain ~1 (see Ref. [15]). In addition, such designs require complex targets with multiple shells and buffer layers to mitigate hydrodynamic instability growth.

The wetted-foam designs have also been considered in the past [16], including designs with liquid DT layers [17]. The latter was proposed to reduce the target convergence ratio by increasing DT vapor density. These designs, however, still require fill tubes and the target gains do not exceed gain ~1.

The proposed new design uses a single foam shell filled with liquid DT to form a fuel sphere (not a layer), but uses the central hot-spot ignition approach instead of volume ignition. This is accomplished by dynamically creating a higher-density fuel shell surrounding a lower-density central region. The design evolution begins by launching a few-Mbar shock wave into the homogeneous fuel. After reflecting from the center and reaching the outer surface of the sphere (ablation front), the shock breaks out of the sphere and the shock-compressed fuel begins to expand outward. Such expansion continues until the fuel pressure reduces below the ablation pressure. Subsequently, a shock is formed near the ablation front, which slows down the fuel expansion, forming a shell. At this point, the shell can be accelerated inward using either the conventional central hot-spot approach or the shock ignition (SI) concept [18]. In other words, the dynamic shell formation can be considered as the target preconditioning stage either for the conventional or SI hot-spot ignition approach.

The stability optimization (described later in the text) leads to a laser-drive pulse consisting of several short-duration intensity pulses (pickets). To explain the basic concept of dynamic shell formation and highlight possible issues, however, it is instructive to consider a simplified design with a continuous drive pulse (without pickets), where constant in time power of $P_L = 1$ TW (Terawatt) is used for the shell-forming part of the design. The target is

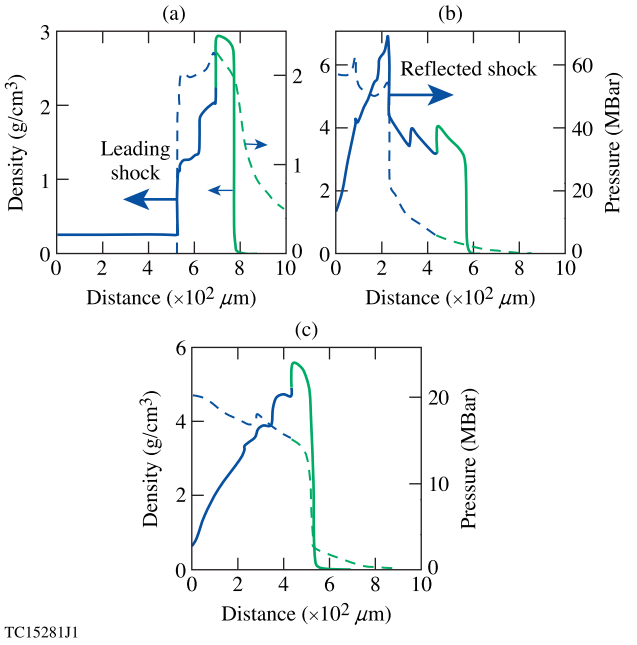

FIG. 1. Snapshots of density (solid lines) and pressure (dashed lines) profiles at (a) $t = 35$ ns, (b) $t = 51$ ns, and (c) $t = 61$ ns. Green and blue lines denote CH and DT, respectfully.

100-μm-thick, 2400-μm-OD solid-density CH shell filled with homogeneous DT fuel. According to 1D simulations using the hydrodynamic code LILAC [19], the ablation pressure corresponding to these drive conditions is $p_a = 2$ Mbar for an on-target overlap incident intensity of $I \simeq 5.5 \times 10^{12}$ W/cm^2. A sequence of hydrodynamic profiles is shown in Figs. 1(a)–1(c). At 35 ns, the shock travels halfway into the DT sphere [see Fig. 1(a)]. Note that an additional DT density jump at $R \simeq 650$ μm is caused by the coalescence of the leading shock wave with the adjustment compression wave created because of fuel-ablator density mismatch. Later, as the leading shock approaches the target center, the shock pressure increases due to its convergence. Figure 1(b) shows a snapshot of the density and pressure profiles at $t = 51$ ns as the shock reflects from the center and travels outward. After reaching several hundred megabars at the center (compared to 2-Mbar ablation pressure), the shock pressure decays down to ~16 Mbar (material at the target center is cooling down at the same time, similar to the blast wave) by the time the reflected shock breaks out of the sphere [$t = 61$ ns, see Fig. 1(c)]. At this point, the shock-compressed material begins to expand outward and, soon after the material pressure drops below the ablation pressure ($p_a \simeq 2$ Mbar), an adjustment compression wave, and later a shock, are formed in the ablator [as shown in Fig. 2(a) at $t = 72$ ns]. The shock moves through the expanding material, compressing it and forming a shell. Positive pressure gradient at the ablation front slows down the shell until its velocity goes through zero and the shell starts to move inward [see Fig. 2(b) showing density and pressure profiles at $t = 110$ ns]. This concludes the

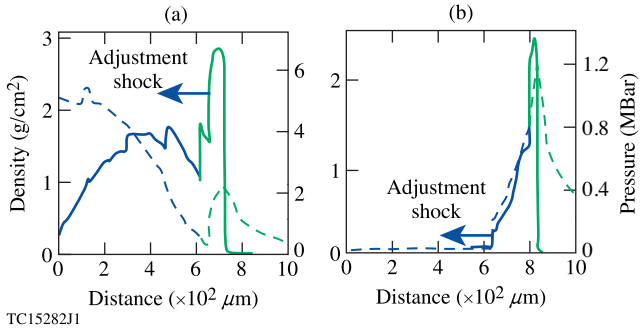

FIG. 2. Snapshots of density (solid lines) and pressure (dashed lines) profiles during the adjustment shock propagation (a) at $t =$ 72 ns and (b) at $t = 110$ ns when shell velocity goes to zero.

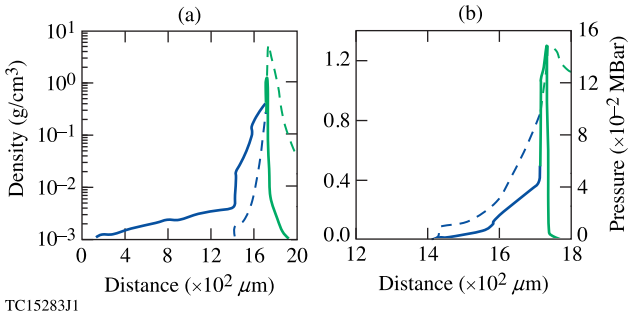

FIG. 3. Dynamically formed shell profiles [(a) linear and (b) logarithmic-density scales, respectively] at $t = 180$ ns for the pulse shown in Fig. 4.

shell-formation phase. At this point the shell can be accelerated toward the center, similar to the conventional or SI ICF hot-spot designs.

One of the critical implosion parameters in the hot-spot ICF ignition designs is the shell implosion velocity $v_{\rm imp}$ (peak in mass-averaged shell velocity). To reach the ignition condition in the conventional designs, the shell must be accelerated to $v_{\rm imp} > 3.5 \times 10^7$ cm/s (see Ref. [2]). Shell momentum conservation defines the relation between the acceleration distance (or initial inner shell radius R_0), shell mass $M_{\rm shell}$, drive (ablation) pressure p_a, and $v_{\rm imp}$ (see, for example, Ref. [20]),

$$R_0 \simeq 1.1 \left(\frac{M_{\rm shell} v_{\rm imp}^2}{4\pi p_a} \right)^{1/3}. \quad (1)$$

In the example under consideration, the unablated shell mass at the beginning of acceleration is $M_{\rm shell} \simeq 2.5$ mg. Substituting $p_a \simeq 200$ Mbar (which is typical for the drive intensity of $I \simeq 10^{15}$ W/cm^2) and $v_{\rm imp} = 4 \times 10^7$ cm/s into Eq. (1) leads to $R_0 \simeq 1300$ μm. The inner radius of the dynamically formed shell shown in Fig. 2(b) is $R_0 \simeq 600$ μm, which is more than twice smaller than the distance necessary to accelerate the shell to the required implosion velocity. The diameter of the dynamically formed shell is controlled by the ablation pressure and therefore, by the laser power. LILAC simulations suggest that reducing the laser power after the first shock reflects from the center to $P_L = 0.3$ TW increases the inner shell radius to $R_0 \simeq$ 1400 μm, close to the estimate provided by Eq. (1). The snapshot of the shell prior to being accelerated is shown in Fig. 3.

Then, the subsequent shell acceleration and fuel compression can be accomplished using either the conventional or SI hot-spot designs. An example of ignition pulse shape that combines the shell-formation part ($t < 180$ ns) and the fuel-acceleration and compression part using the conventional hot-spot ignition concept ($t \geq 180$ ns) is shown in Fig. 4. The total pulse energy is 1.15 MJ. The acceleration part of the pulse has a continuous, 25-ns rise from 0.3 TW to 250 TW. The design reaches $v_{\rm imp} = 3.5 \times 10^7$ cm/s, and, when alpha deposition is not included in the calculation, the peak areal density reaches $\rho R_{\rm peak} \simeq 2$ g/cm^2 and peak neutron-average pressure is 220 Gbar. When alpha deposition is included, the target ignites and gives 1D gain = 75.

The target design using the solid-density CH shell driven by the pulse shown in Fig. 4, although conceptually simple, has several undesirable features. First, the contrast ratio of the main pulse is rather high, 830, which makes it challenging to implement using existing laser technologies. Second, 3D simulations using the hydrodynamic code ASTER [21] show that a 50-ns-long, low-intensity drive is causing very high secular growth (linear and quadratic in time) of long- and intermediate-wavelength modes ($\ell < 20$) due to power imbalance, target offset, and beam geometry. In addition, the conduction zone at $t = 72$ ns (see Fig. 2), when the shell-forming shock is launched into the fuel, is very short, causing growth of the short- and intermediate-scale nonuniformity seeded by single-beam speckle pattern and beam geometry. The problem is exacerbated by the fact that the initial target radius (1200 μm) is substantially smaller than the outer radius of the dynamically formed shell at the beginning of acceleration [$R_{\rm out} \simeq 1700$ μm, as

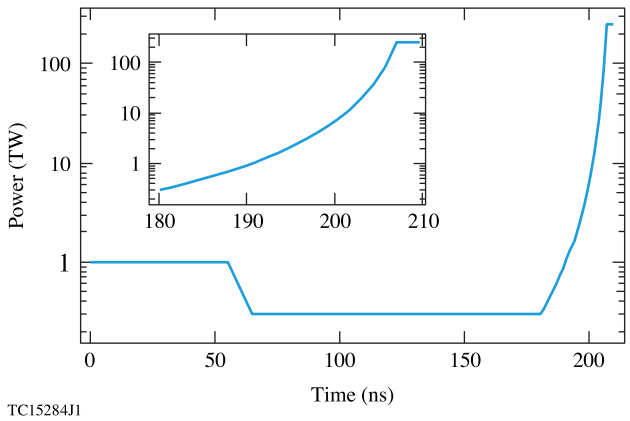

FIG. 4. Pulse shape for the $E_L = 1.15$-MJ ignition dynamic-shell design. The inset shows the main drive pulse.

shown in Fig. 3(a)], leading to reduced beam overlap and enhanced drive nonuniformity.

One possible mitigation strategy for the excessive nonuniformity growth is to increase the number of laser beams and to make the individual beam focal spots bigger. This enhances the overlap intensity uniformity and reduces the nonuniformity seeding. Another solution is to increase target robustness by replacing the long, low-intensity part of the drive with several intensity pickets, similar to adiabat shaping designs currently used in ICF implosions [22]. This minimizes growth of long-wavelength modes and, as recently demonstrated [23], significantly reduces laser imprint (because of the hydrodynamic flow directed from a decaying shock toward the ablation front). To address the short-scale perturbation growth and mix at the ablator-DT interface, the solid-density CH shell must be replaced with a low-density ($\rho \sim 0.1$ g/cm^3 or lower) foam wicked with DT (wetted foam). This minimizes the Atwood number at the interface during propagation of decaying shocks launched by the intensity pickets. The pressure and density gradients behind these shocks have opposite directions at the interface, leading to the RT instability growth. Hence, replacing solid-density CH with the foam significantly reduces the growth factors of the unstable modes at the interface. Reducing the ablator density also increases the initial target size from 1200 to 1500 μm (keeping the target mass approximately the same), nearly matching the shell radius R_{out} at the beginning of acceleration phase. This allows the design to use the larger drive beams, improving overlap laser-intensity uniformity at the shell formation as well as shell acceleration phases.

The liquid DT spheres with foam shells are especially beneficial for the target production for inertial fusion energy (IFE). Such designs eliminate the necessity for fuel layering and the fill tube. The desired quantity of DT can be added to the target using two methods. The first is the process used to permeation fill current cryogenic targets where a predetermined mass of gas is condensed in a volume containing the foam shell, and then use capillary force to wick the liquid into the shell [24]; the second uses electrocapillary forces to form a droplet of liquid and move it into contact with a foam shell, again relying on capillary forces to wick the fuel into the target [25]. The process of injecting a target to the reactor center for the IFE application was discussed in Ref. [26]. A target injector system with a magnetic sabot remover was developed as part of the high average power laser (HAPL) program [26]. Several technical issues still remain (such as keeping the target in a saturated DT vapor environment to prevent liquid DT from evaporating from the target) and will be addressed in the future work.

Two examples of the pulse shapes with intensity pickets used to drive liquid DT foam targets are shown on Figs. 5(a) and 5(b). These designs use 0.5-ns pickets; however, the picket duration can be different as soon as the strength of the launched shocks is kept constant. The first

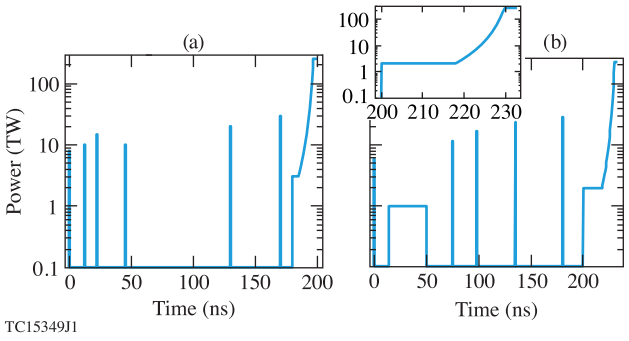

FIG. 5. (a) Picket-pulse, dynamic-shell designs with the multiple pickets and (b) a picket and continuous drive options for the shock transit phase through a homogeneous fuel sphere.

three pickets shown in Fig. 5(a) send shocks that coalesce near the target center. The number of shocks launched earlier in the pulse is determined by requiring minimization of the fuel adiabat in the outer region of the sphere (which contributes later to the fuel shell) while providing enough shock heating close to the target center (which will form a low-density region inside the shell). The merged shocks raise the adiabat and provide momentum and internal energy to the central region sufficient to expand the material and reduce its density below $\rho \sim 10^{-3}$ g/cm^3. As an alternative approach, instead of sending multiple decaying shocks, this can be accomplished by a single decaying shock followed by a low-intensity (a few 10^{12} W/cm^2), 30-ns drive. Such a design is shown in Fig. 5(b). Then, three to four pickets at later times are used to slow down the expanding ablator and fuel material and to launch a shock that compresses the fuel and forms a shell, similar to the continuous-pulse design shown in Fig. 4. One key difference of the picket design, in comparison with the continuous-pulse design, is that the shell-forming shocks are launched further out in the corona (because of longer-density scale length), preventing coupling of the laser nonuniformities (speckles) to the main fuel and, therefore, reducing seeding to the RT instability developed during shell acceleration. Launching several decaying shocks prior to the main pulse in the picket designs shown in Figs. 5(a) and 5(b) also reduces the contrast ratio of the main pulse (from 830 for the continuous pulse down to ~100 in the picket designs), significantly reducing the dynamic range of the required laser power.

To study the target response to low- and intermediate-mode ($\ell < 20$) drive nonuniformities in the foam design driven by picket pulses, several 3D ASTER simulations were performed. They demonstrated superior target uniformity during the shell formation and shell acceleration phases compared to the continuous-pulse design. Although these preliminary results are encouraging, more work is needed to address the target robustness against short-scale perturbations seeded by target roughness and laser imprint. Such analysis requires computationally intense,

high-resolution 3D simulations, which are currently under way. This work will be discussed in future publications. In addition, the future sensitivity studies and experiments will address the accuracy requirements for equation-of-state and other material properties for DT and wetted foams, since timing multiple shocks in the picket designs might be challenging in the experiments.

In summary, a new class of ignition designs is proposed for ICF experiments. These designs are based on the hot-spot ignition approach and use a liquid DT sphere inside a wetted-foam shell to form the lower-density central region and the higher-density shell dynamically by appropriately shaping the laser pulse. The pulse shapes for the new designs range from continuous to multiple-picket designs. Preliminary 3D simulations of the continuous-pulse designs indicate high growth of long-wavelength modes caused by beam imbalance, target offset, and beam geometry. The picket-pulse designs, on the other hand, have been shown to be more robust against such nonuniformity growth. Detailed stability analysis and material-properties sensitivity studies of the dynamic-shell designs will be discussed in future publications.

This material is based upon work supported by the Department of Energy National Nuclear Security Administration under Award No. DE-NA0003856, the University of Rochester, and the New York State Energy Research and Development Authority. This report was prepared as an account of work sponsored by an agency of the U.S. Government. Neither the U.S. Government nor any agency thereof, nor any of their employees, makes any warranty, express or implied, or assumes any legal liability or responsibility for the accuracy, completeness, or usefulness of any information, apparatus, product, or process disclosed, or represents that its use would not infringe privately owned rights. Reference herein to any specific commercial product, process, or service by trade name, trademark, manufacturer, or otherwise does not necessarily constitute or imply its endorsement, recommendation, or favoring by the U.S. Government or any agency thereof. The views and opinions of authors expressed herein do not necessarily state or reflect those of the U.S. Government or any agency thereof.

[1] J. D. Lindl, *Inertial Confinement Fusion* (Springer, New York, 1998).
[2] S. Atzeni and J. Meyer-Ter-Vehn, *The Physics of Inertial Fusion* (Clarendon Press, Oxford, 2004).
[3] O. A. Hurricane, P. T. Springer, P. K. Patel *et al.*, Phys. Plasmas **26**, 052704 (2019).
[4] V. Gopalaswamy, R. Betti, J. P. Knauer *et al.*, Nature (London) **565**, 581 (2019).
[5] D. S. Clark, C. R. Weber, and A. L. Kritcher *et al.*, Nucl. Fusion **59**, 032008 (2019).
[6] S. Chandrasekhar, *Hydrodynamic and Hydromagnetic Stability* (Claredon, Oxford, 1961), p. 428.
[7] S. W. Haan, J. D. Lindl, D. A. Callahan *et al.*, Phys. Plasmas **18**, 051001 (2011).
[8] J. K. Hoffer and L. R. Foreman, Phys. Rev. Lett. **60**, 1310 (1988).
[9] P. W. McKenty, V. N. Goncharov, R. P. J. Town, S. Skupsky, R. Betti, and R. L. McCrory, Phys. Plasmas **8**, 2315 (2001).
[10] S. X. Hu, V. N. Goncharov, P. B. Radha, J. A. Marozas, S. Skupsky, T. R. Boehly, T. C. Sangster, D. D. Meyerhofer, and R. L. McCrory, Phys. Plasmas **17**, 102706 (2010).
[11] V. N. Goncharov, S. Skupsky, R. T. Boehly, J. P. Knauer, P. McKenty, V. A. Smalyuk, R. P. J. Town, O. V. Gotchev, R. Betti, and D. D. Meyerhofer, Phys. Plasmas **7**, 2062 (2000).
[12] D. S. Montgomery, W. S. Daughton, B. J. Albright *et al.*, Phys. Plasmas **25**, 092706 (2018).
[13] S. X. Hu, R. Epstein, and W. Theobald *et al.*, Phys. Rev. E **100**, 063204 (2019).
[14] K. Molvig, M. J. Schmitt, B. J. Albright, E. S. Dodd, N. M. Hoffman, G. H. McCall, and S. D. Ramsey, Phys. Rev. Lett. **116**, 255003 (2016).
[15] M. Rosen, Phys. Plasmas **6**, 1690 (1999).
[16] T. J. B. Collins, J. A. Marozas, R. Betti, D. R. Harding, P. W. McKenty, P. B. Radha, S. Skupsky, V. N. Goncharov, J. P. Knauer, and R. L. McCrory, Phys. Plasmas **14**, 056308 (2007).
[17] R. E. Olson, R. J. Leeper, J. L. Kline *et al.*, Phys. Rev. Lett. **117**, 245001 (2016).
[18] R. Betti, C. D. Zhou, K. S. Anderson, J. L. Perkins, W. Theobald, and A. A. Solodov, Phys. Rev. Lett. **98**, 155001 (2007).
[19] J. Delettrez, R. Epstein, M. C. Richardson, P. A. Jaanimagi, and B. L. Henke, Phys. Rev. A **36**, 3926 (1987).
[20] V. N. Goncharov, T. C. Sangster, R. Betti *et al.*, Phys. Plasmas **21**, 056315 (2014).
[21] I. V. Igumenshchev, V. N. Goncharov, F. J. Marshall *et al.*, Phys. Plasmas **23**, 052702 (2016).
[22] V. N. Goncharov, T. C. Sangster, T. R. Boehly *et al.*, Phys. Rev. Lett. **104**, 165001 (2010).
[23] I. V. Igumenshchev, A. L. Velikovich, V. N. Goncharov, R. Betti, E. M. Campbell, J. P. Knauer, S. P. Regan, A. J. Schmitt, R. C. Shah, and A. Shvydky, Phys. Rev. Lett. **123**, 065001 (2019).
[24] R. A. Sacks and D. H. Darling, Nucl. Fusion **27**, 447 (1987).
[25] T. B. Jones, R. Gram, K. Kentch, and D. R. Harding, J. Phys. D **42**, 225505 (2009).
[26] J. D. Sethian, A. R. Raffray, J. Latkowski, J. P. L. Snead, T. J. Renk, and S. Sharafat, J. Nucl. Mater. **347**, 161 (2005).